Second Quarterly Progress Report,
Covers Period 17 August 1962 to 16 November 1962

t. "A STEADY STATE HALL CURRENT ACCELERATOR" 2d Quarterly . . .

Prepared for
National Aeronautics and Space Administration
Lewis Research Center
21000 Brookpark Road
Cleveland 35, Ohio

(NASA Contract ~~No.~~ NAS 3-2500)
(EOS ~~Report~~ 3160-Q-2) Final OTS

14 December 1962

Prepared by

Gordon L. Cann

1. G. L. Cann,
Principal Investigator

and

2. G. L. Marlotte, and
3. R. W. Ziemer

Dec. 14, 1962 43p refs

Approved by

John M. Teem

John M. Teem, Manager
FLUID PHYSICS DIVISION

2 90400 1

ELECTRO-OPTICAL SYSTEMS, INC., PASADENA, CALIFORNIA

CONTENTS

## LIST OF FIGURES

## 1. SUMMARY

The basic theory of Hall current accelerators and generators is rederived in this quarterly report. Considerable effort is devoted to keeping the results as general as is possible. Attempts are made to find the physical significance of the resulting equations so that a good basic understanding of the mechanisms involved can be obtained. The parameters that appear are written in terms of quantities that can be measured and over which some control can be exercised in setting up and operating an accelerator.

Some rather modest assumptions are made so that the terms representing the momentum and energy transferred to the gas from the electromagnetic field can be simplified to permit a gas dynamic analysis to be made. The gas dynamic studies indicate that arbitrarily high velocity ratios are obtainable across a Hall accelerator, but that the gas is also heated to very high temperatures. Curves indicating the efficiency with which the device can accelerate the gas are presented and indicate that in order to obtain efficiencies of over 60%, it is necessary to increase the gas velocity by over a factor of 6.

Considerable experimental progress has been made during this last quarter. In order to keep a current filament from forming down the axis of the accelerating channel, a centre body has been introduced. It has been found that an iron centre body improved the distribution of the radial magnetic field component so that considerably better performance is obtained from the accelerator. A graphite second cathode has been used and allowed to run hot. Some cathode erosion occurred and the discharge was observed to still attach at a point under some operating conditions.

When the iron centre body was used, a series of tests were conducted to try and verify some of the theoretical predictions. The force per unit volume transmitted to the gas was found to become independent of the magnetic field as the field strength was increased from zero to several thousand gauss; the current in the discharge being held constant. The potential drop across the accelerator has also been increased by a factor of over 3 by increasing the accelerator magnet field strength from zero to several thousand gauss.

It is now felt that the concept of Hall acceleration has been proved experimentally to be valid. It has been further shown experimentally that the relationship predicted by theory between the magnetic field strength, the electric field and the momentum transferred to the gas exist to within a reasonable degree of accuracy. Because of this correlation between theory and experiment, it is now feasible to design a high specific impulse, fairly high efficiency accelerating device from the extensive gas dynamic analysis that we have done.

## 2. INTRODUCTION

Initial investigations of the mechanisms that occur in a Hall current accelerator were conducted analytically using only a current density equation. Such studies cannot give any of the details of the ion or electron motion, but only their combined effect. In order to obtain a clear picture of the energy and momentum transfer processes it is hence desirable to study the equations describing the electron and ion motion separately. This has been done and the results are shown in this report. Clearly, these results do not negate those reported in the first quarterly report, they merely amplify them and give more detail of the physical processes that are occurring in the accelerator.

Some attempts have been made in the past to determine the efficiency of the accelerating process. These calculations involved making a number of fairly unwarranted assumptions, hence the results were open to question. In order to obtain an accurate evaluation of the thrust efficiency of the accelerator, it is necessary to make a gas dynamic study of the process. This has been done with considerable generality and the results are reported here.

Several major modifications have been made to the experiment in order to improve the acceleration process. A hot hollow cathode has been designed, fabricated and tested. Since the physical processes that occur in such a cathode are not well understood, the design was somewhat arbitrary and the present performance indicates that modifications need to be made in order to improve the uniformity of current density over the surface area.

Tests reported previously indicated that a current filament formed along the axis of the accelerator when the channel was open. Introducing a centre body, forming an annulus for the gas to flow in, has resulted in great improvements in the performance of the accelerator. The results obtained when using both an insulated copper and an insulated iron centre body are reported here.

## 3. ANALYSIS

### 3.1 Momentum and Energy Transfer Mechanisms

In this section the components of electron and ion diffusion are solved for in a very general manner. The expressions that are obtained can be used to determine the physical processes that are occurring in a Hall current accelerator.

#### 3.1.1 Ion and Electron Diffusion Equations

A model of the Hall accelerator will be used that consists of an annulus across which a radial magnetic field is applied.* Current will be drawn through the annulus by applying an electric field between electrodes placed at either end of the annulus. In this model, there is no radial force applied to the gas, hence radial components of mass motion and diffusion are considered to be zero. The induced tangential magnetic field due to the axial current will be assumed negligible with respect to the applied magnetic field. Thermoelectric potentials are also considered to be negligible. The coupled equations for the ion and electron diffusion in a partially ionized gas are now given by:**

$$(1 + \beta_1)\, u_e - u_I = - \gamma \left[ (1 + \beta_1)\, (\epsilon + \beta) - \epsilon \right] \left[ F_1 + u_e \times B \right] \tag{1}$$

$$-\epsilon\, u_e + (\epsilon + \beta)\, u_I = \gamma \left[ (1 + \beta_1)\, (\epsilon + \beta) - \epsilon \right] \left[ F_1 + u_I \times B \right] \tag{2}$$

where $\epsilon = n_e / n_I$

---

* See Fig. 1

** See Ref. 2

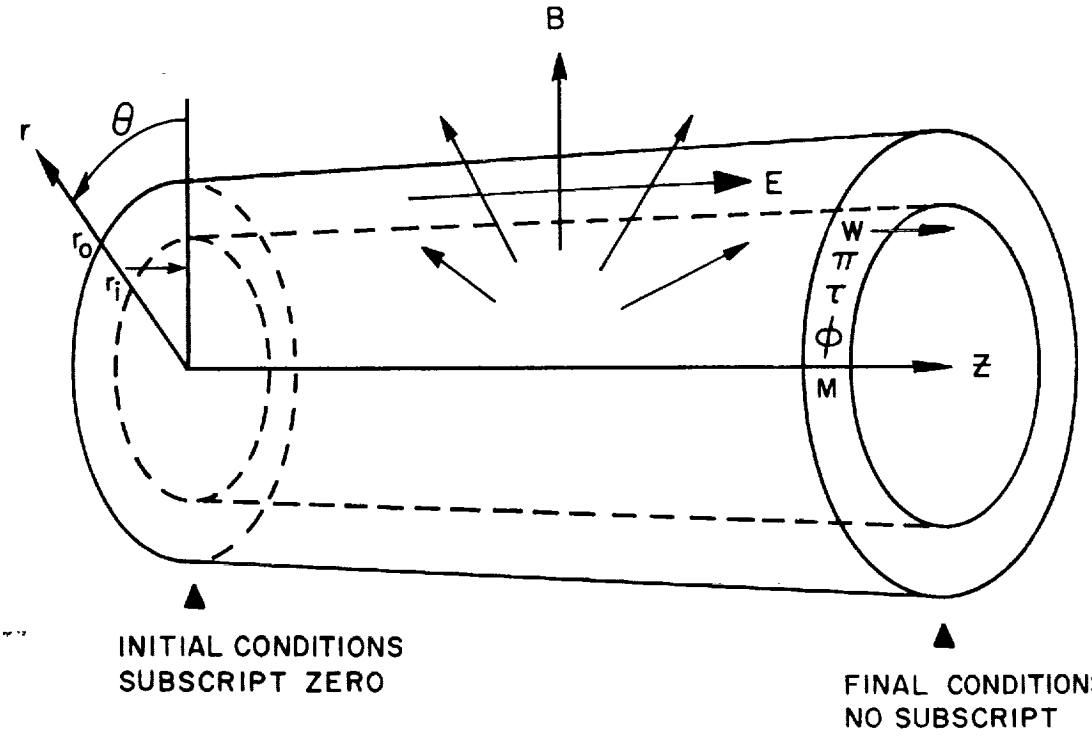


$$W = \frac{w}{w_0} \quad \pi = \frac{P}{P_0}$$

$$\tau = \frac{T}{T_0} \quad \phi = \left(\frac{\gamma}{\gamma - 1}\right)\frac{\alpha |e| \dot{m}}{m_i I}$$

ASSUMPTIONS:

$$\frac{r_o - r_i}{r_o} << 1$$

B = CONSTANT

ALL QUANTITIES MAY BE "AVERAGED" OVER THE ANNULUS

$$\frac{\partial}{\partial t} = \frac{\partial}{\partial r} = \frac{\partial}{\partial \theta} = 0$$

AZIMUTHAL VELOCITY V << W

FIG. 1 GEOMETRY OF MODEL AND ASSUMPTIONS

$$(1 + \beta_1)\,\gamma = \frac{\omega_I \tau_I}{|B|} = \frac{\psi_I}{|B|}$$

$$\beta\ \gamma = \frac{\omega_e \tau_e}{|B|} = \frac{\psi_e}{|B|}$$

$$F_1 = E + u \times B.$$

General expressions for the diffusion velocity components can be obtained from Eqs. (1) and (2). However, these are so general that little can be learned from them without some assumptions. Initially, we shall assume that no charge concentration occurs, e.g. $\epsilon = 1$, and also that $\beta \gg \beta_1$. This last assumption can be rewritten as:*

$$\frac{(n_I + n_a)^2}{n_a^2}\ \frac{q_{Ia}}{q_{ea}}\ \left(\frac{2m_a}{m_e}\right)^{1/2} \gg 1$$

where $q_{Ia}$ and $q_{ea}$ are the collision cross sections between ions and atoms, and between electrons and atoms, respectively. Because of the mass ratio term, this assumption is justified over the whole range of partial ionization.

The axial components are electron and ion diffusion and can now be written as:

$$\left[(1 + \psi_e\psi_I)^2 + \psi_e^2\right] w_e = -\beta\,(1 + \frac{\beta_1}{1+\beta_1}\,\psi_I^2)\,\gamma\,(E_z - vB) - (1 + \psi_I^2)\,\psi_e^2\,w \tag{3}$$

$$\left[(1 + \psi_e\psi_I)^2 + \psi_e^2\right] w_I = \beta\,\psi_I\psi_e\,\gamma\,(E_z - vB) - \left[1 + (1+\beta_1)\,\psi_e\psi_I\right]\psi_e\,\gamma\,w\,B \tag{4}$$

---

* See Ref. 2

These expressions can be combined to give the axial current density

$$\frac{j_z B}{|e| n_I} = \frac{\psi_e (1 + \psi_e \psi_I) (E_z - vB) + \psi_e^2 wB}{\psi_e^2 + (1 + \psi_I \psi_e)^2} \tag{5}$$

A number of observations can be made from these equations.

1.) Equations 3, 4, 5 are symmetric in the magnetic field, except for the vB terms, so that reversing the magnetic field has no effect on them.

2.) The axial current density tends to concentrate where the axial velocity is highest and when ion density is highest. This keeps the current out of the boundary layers that form along the inner and outer walls and hence insure that a high percent of the energy and momentum is transferred to the gas from the electromagnetic field rather than directly to the boundary layers and thence readily to the walls.

3.) When the magnetic field is strong enough so that $\psi_I \psi_e \gg 1$, then, from Eq. (3) the electron diffusion velocity becomes very closely the reverse of the gas velocity, e.g. the electrons are effectively trapped by the magnetic field and remain stationary in space. This then indicates that the current density can be written as

$$j = |e| n_I (w + w_I) \tag{6}$$

This equation implies that the current is carried by the absolute velocity $(w + w_I)$ of the ions in space.

Expressions, similar to the above, can be obtained for the tangential components of diffusion for the electrons and ions.

$$\left[(1 + \psi_e \psi_I)^2 + \psi_e^2\right] v_e = \beta^2 (1 + \psi_I^2) \gamma B (E_z - vB) - (1 + \frac{\beta_1}{1+\beta_1} \psi_I^2) \psi_e w \tag{7}$$

$$\left[(1 + \psi_e\psi_I)^2 + \psi_e^2\right] v_I = \left[1 + (1 + \beta_1)\ \psi_e\psi_I\right] \psi_e\ (E - vB) + \psi_e^2\ \psi_I\ w \tag{8}$$

The tangential current density equation becomes:

$$\frac{j_\theta\ B}{|e|\ n_I} = -\left\{\frac{\psi_e^2\ (E_z - vB) - \psi_e\ (1 + \psi_e\psi_I)\ wB}{(1 + \psi_e\psi_I)^2 + \psi_e^2}\right\} \tag{9}$$

Using Eq. (5) the expression $E_z - vB$ can be eliminated from Eq. (9) to give

$$\frac{j_\theta\ B}{|e|\ n_I} = \frac{\psi_e B}{1 + \psi_e\psi_I}\left(\frac{j_z}{|e|\ n_I} - w\right) \tag{10}$$

A number of important and interesting conclusions can be drawn from these equations:

1.) Equations 7, 8 and 9 are antisymmetric in the magnetic field so that the tangential currents reverse when the magnetic field is reversed.

2.) The tangential current density tends to be spread away from the regions of high velocity. This effect acts as a stabilizing influence on the gas velocity during acceleration and helps to form a core of gas with uniform axial velocity outside of the boundary layer.

### 3.1.2 The Applied Electric Field Strength

Equations 3, 4, and 5 indicate that when the magnetic field is small the current is carried by electrons primarily and the electric field is relatively small.

$$E_z = j_{z/a} = \frac{I}{\sigma A} \tag{11}$$

However, as the magnetic field is increased, the electric field increases enough to cause appreciable ion slip so that a significant portion of the current is now carried by the ions. When $\psi_e \psi_I \gg 1$, then the electric field becomes

$$E_z - vB = \frac{(1 + \psi_I^2)}{|e| n_I} \frac{j_z B}{\psi_I} - \frac{w B}{\psi_I} \tag{12}$$

$$= \frac{I}{\sigma A} \left[ \frac{\psi_e}{\psi_I} \left\{ (1 + \psi_I^2) - \frac{|e| n_I w}{j} \right\} \right]$$

As long as the quantity $\frac{|e| n_I w}{j}$ is not too close to the value 1, then an appreciable increase in the electric field results from the application of the radial magnetic field.

If the velocity and ion density are fairly constant over the cross section, the quantity $\frac{|e| n_I w}{j}$ can be written in terms of parameters over which we have some control;

$$\frac{|e| n_I w}{j} = \frac{\dot{m} |e| \alpha}{I m_a} = \psi \tag{13}$$

If the gas remained in equilibrium and if it were possible to determine the gas temperature, then it would be possible to evaluate $\psi$ in terms of measured quantities and thus evaluate the value of E - vB, which is essentially the applied electric field as long as the tangential gas velocity remains small. What is perhaps more important is the fact that it should be possible to control the applied electric field strength by changing any one of: the mass flow rate, the electric current or the gas temperature. In practice, when a current is drawn through a fairly low pressure gas, the ionization level does not stay in equilibrium and some relation between j and $n_I$ exists. This makes it almost impossible

to predict the electric field strength that will result due to the application of the magnetic field. However, once $\psi_e\psi_I \gg 1$ and if v is small, then the electric field is independent of the magnetic field strength and it should be possible to determine the relation between j and $n_I$ from a measurement of $E_z$, provided the values of $\sigma$ and $\psi_e/\psi_I$ can be determined.

3.1.3 The Force Equations

The tangential force that the gas experiences is given by:

$$\frac{X_\theta}{|e|\, n_I} = \frac{\psi_e\,(1 + \psi_e\psi_I)\,(E_z - vB) + \psi_e^{\,2}\, wB}{\psi_e^{\,2} + (1 + \psi_I\psi_e)^2} \tag{14}$$

The axial force that is applied to the gas is expressed by:

$$\frac{X_z}{|e|\, n_I} = \frac{\psi_e^{\,2}(E_z - vB) - \psi_e\,(1 + \psi_e\psi_I)\,wB}{\psi_e^{\,2} + (1 + \psi_I\psi_e)^2} = \frac{\psi_e\, B}{1 + \psi_e\psi_I}\left(\frac{j_z}{|e|\, n_I} - w\right) \tag{15}$$

The ratio of these two forces can be expressed by:

$$\frac{X_\theta}{X_z} = \frac{1 + \psi_e\psi_I}{\psi_e}\left(1 - \frac{|e|\, n_I\, w}{j}\right) \tag{16}$$

Equation 14 indicates that the tangential force reverses as the applied radial magnetic field reverses. Equation 16 shows that there are two regimes in which it is possible to have $X_\theta/X_z \ll 1$. This is when $\psi_e < 1$, and when $\psi_e\psi_I \gg 1$ but $\psi_I < 1$. In the first regime, where $\psi_e < 1$, the force experienced by the gas is quite small and depends quadratically on the magnetic field strength. The second regime, where $\psi_e\psi_I \gg 1$ and

$\psi_I < 1$, is the more desirable region in which to operate, since much larger forces per unit volume are transmitted to the gas and the force becomes independent of the applied magnetic field strength. In order to have $\psi_e\psi_I \gg 1$ and $\psi_I < 1$, the ratio $\psi_I/\psi_e$ should be made as small as possible. This ratio can be written as:*

$$\frac{\psi_I}{\psi_e} = \left(\frac{2\ m_e}{m_a}\right)^{1/2} \quad \frac{n_I\ q_{eI}/f_{eI}^{(2)} + n_a\ q_{ea}/f_{ea}^{(2)}}{(n_I + n_a)\ q_{Ia}/f_{Ia}^{(2)}} \quad \frac{n_a}{n_a + n_I} \tag{17}$$

In order to make this ratio large, the particle atomic weight should be large, the electron temperature should be high, and the ionization level should be either quite low or quite high. Equation 15 indicates that the direction of the axial force that the gas experiences is independent of the magnitude and polarity of the radial magnetic field. It further shows that the axial force depends quadratically on the magnetic field strength for small magnetic fields and when $\psi_e\psi_I > 1$, the axial force becomes independent of the magnetic field strength.

When the magnetic field is strong enough so that $\psi_e\psi_I \gg 1$, then

$$X_z = \frac{I\ B}{A\ \psi_I}\left(1 - \frac{\dot{m}\ |e|\ \alpha}{I\ m_a}\right) = \frac{I\ B}{A\ \psi_I}\ (1 - \psi) \tag{18}$$

where $\psi = \dfrac{\dot{m}\ |e|\ \alpha}{I\ m_a}$ = ratio of the charge carried by the ion motion, to the total electric current. In deriving Equation (11) it has been assumed that the gas velocity and ion density were fairly uniform over the cross-section. It must be emphasized that when the gross parameters of mass flow rate, current, and ionization level indicate that $\psi > 1$, then Equation 11 is no longer valid. It has previously been postulated (see first quarterly report)** that the condition $\psi = 1$ defined a critical

* See Ref. 3
** See Ref. 1

current, such that a decelerating force was applied to the gas when $\psi>1$. The equation for local conditions, i.e. Eq. (10), indicates, however, that what would probably occur is that current filaments would develop when the average properties of the flow made $\psi>1$. For the accelerator then, we now postulate that the condition $\psi > 1$ is a criterion for the development of current filaments in the axial current flow. The current density will then always remain high enough, so that locally, the current density will be higher than the charge flux due to the ion motion defined by $|e|\, n_I\, w$.

Another way to write the force equation is to replace $\frac{j_z}{|e|\, n_I}$ by $w_I + w$ when $\psi_e \psi_I > 1$. (See Eq. (6)). Equation (10) then becomes:

$$X_z = \frac{|e|\, n_I\, B}{\psi_I}\, w_I \tag{19}$$

This equation says that the force per unit volume applied to the gas is directly proportional to the ion slip.

### 3.2 Gas Dynamics of the Hall Accelerator

In order to obtain some indication of the efficiency of conversion of electric power to effective jet power, a complete gas dynamic solution is necessary. Such a solution also gives a great deal more information. Usually, several non-dimensional parameters appear in the equations that determine the nature of the integral curves. The solution indicates the best values of these parameters to use for any specific application. Critical limits of some quantities almost always appear as well as in the solutions, due to the non-linear nature of the differential equations.

For the above reasons it is often desirable to make some simplifying assumptions in order to get some complete gas dynamic solutions. The assumptions necessary in studying the Hall current accelerator are discussed below.

### 3.2.1 Assumptions Necessary to Obtain a Gas Dynamic Solution

The effects of wall shear stress due to viscosity and of heat loss due to thermal conduction at the wall will be neglected. It will also be assumed that most of the gas mass flows through the annulus in such a manner that gas dynamic properties can be averaged over the channel width. We shall also assume that the accelerator is operating in a range where $X_{\theta/X_z} \ll 1$. Initially it will be assumed that the acceleration is occurring in a constant area channel. The equations of conservation of momentum and energy now become:

$$\frac{d}{dz}\left(p + \rho w^2\right) = \frac{\psi_e B}{1 + \psi_e \psi_I} \frac{I}{A} (1 - \psi) \tag{20}$$

$$\frac{d}{dz}\left\{\rho w \left(h + \frac{w^2}{2}\right)\right\} = \frac{w B \psi_e}{\psi (1 + \psi_e \psi_I)} \frac{I}{A} \left\{1 - \psi + \left(\frac{1 + \psi_e \psi_I}{\psi_e}\right)^2\right\} \tag{21}$$

When these two equations are combined, the following expression results:

$$\frac{d}{dz}\left\{\rho w \left(h + \frac{w^2}{2}\right)\right\} = \frac{w}{\psi} \left\{\frac{1-\psi + \left(\frac{1 + \psi_e \psi_I}{\psi_e}\right)^2}{1 - \psi}\right\} \frac{d}{dz}\left(p + \rho w^2\right) \tag{22}$$

We shall next assume that over the range that the solution is valid $\left(\frac{1 + \psi_e \psi_I}{\psi_e}\right)^2 \ll 1-\psi$, and that $\psi$ is a constant. These assumptions are identically valid for a fully ionized gas in which: i) the percent ionization is frozen at a constant value through the accelerator, and ii) the value of $(\omega_I \tau_I)^2 \ll 1$. The above assumptions reduce Eq. (22) to the following expression:

$$d\left\{\rho w\left(\frac{\gamma}{\gamma-1}\frac{p}{\rho}+\frac{w^2}{2}\right)\right\} = \frac{w}{\psi}\, d\,(p+\rho w^2) \tag{23}$$

where $\psi$ is a constant, having a value of less than one.

3.2.2 Differential Equations for the Hall Current Accelerator

A number of differential relations can be obtained from Eq. (23), that are useful in outlining the general performance characteristics of a Hall device. These are given below in terms of the parameters of Mach number M, specific heat ratio $\gamma$, and the quantity $\psi$ or $\Phi = \frac{\gamma}{\gamma-1}\psi$

$$\frac{w}{p}\frac{dp}{dw} = \frac{\Phi(1-M^2) - \gamma M^2(1-\psi)}{1-\Phi} \tag{24}$$

$$\frac{w}{M}\frac{dM}{dw} = \frac{1}{2}\,\frac{2(1-\Phi)\left(1+\frac{\gamma-1}{2}M^2\right) - (1-M^2)}{1-\Phi} \tag{25}$$

$$w\frac{d\left(S/R\right)}{dw} = \frac{\gamma}{\gamma-1}(1-\psi)\,\frac{1-M^2}{1-\Phi} \tag{26}$$

$$M\frac{d\left(S/R\right)}{dM} = \frac{2\gamma}{\gamma-1}\,\frac{(1-\psi)(1-M^2)}{2(1-\Phi)\left(1+\frac{\gamma-1}{2}M^2\right) - (1-M^2)} \tag{27}$$

$$\frac{w}{T}\frac{dT}{dw} = \frac{(1-M^2) - (1-\psi)(\gamma-1)M^2}{1-\Phi} \tag{28}$$

where

$$\Phi = \frac{\gamma}{\gamma-1}\psi$$

$$1 > \psi > 0$$

Using Equations 25, 26, and 27 it is possible to block out regimes in the plane of M vs. $\Phi$ where various processes are occurring. These are shown in Fig. 2. Momentum and energy are added to the gas along lines of constant $\Phi$ for $\Phi < \frac{\gamma}{\gamma-1}$ (accelerator mode) and are removed from the gas along lines of constant $\Phi$ for $\Phi > \frac{\gamma}{\gamma-1}$ (generator mode). Of the six regimes outlined in the accelerator region, the one in which both Mach number and velocity increase during supersonic acceleration appears the most desirable. When operating in this region, a limiting Mach number is approached at the outlet, but the velocity can be made arbitrarily high. This is a very important result, and indicates that there is no inherent upper limit to the velocity that is obtainable due to gas dynamic considerations. Viscous and heat conduction effects will modify this conclusion somewhat, hence the Reynolds number is likely to be the significant parameter in determining the upper limit of velocity obtainable by a gas confined in an annular Hall accelerator.

In Fig. 3, curves are shown along which the temperature and pressure derivatives with respect to the velocity are zero. Between the Mach number 1 line and these curves the temperature and pressure have been continually falling during the acceleration. Between these curves and the limit Mach number curve the temperature and pressure rise.

### 3.2.3 Integral Relations for the Hall Accelerator

The differential relations shown by Equations 24 to 28 can be integrated, the results are shown below:

$$\frac{M_o^2}{M^2} = 1 + \left\{1 - \frac{(1-\psi)\,\gamma\,M_o^2}{2\Phi-1}\right\} \frac{1}{W\,\frac{2\Phi-1}{\Phi-1}} - \left\{1 - \frac{(1-\psi)\,\gamma\,M_o^2}{2\Phi-1}\right\} \tag{29}$$

$$\frac{P}{P_o} = \pi = W\,\frac{M_o^2}{M^2} \tag{30}$$

$$\frac{T}{T_o} = \pi\,W = W^2\,\frac{M_o^2}{M^2} \tag{31}$$

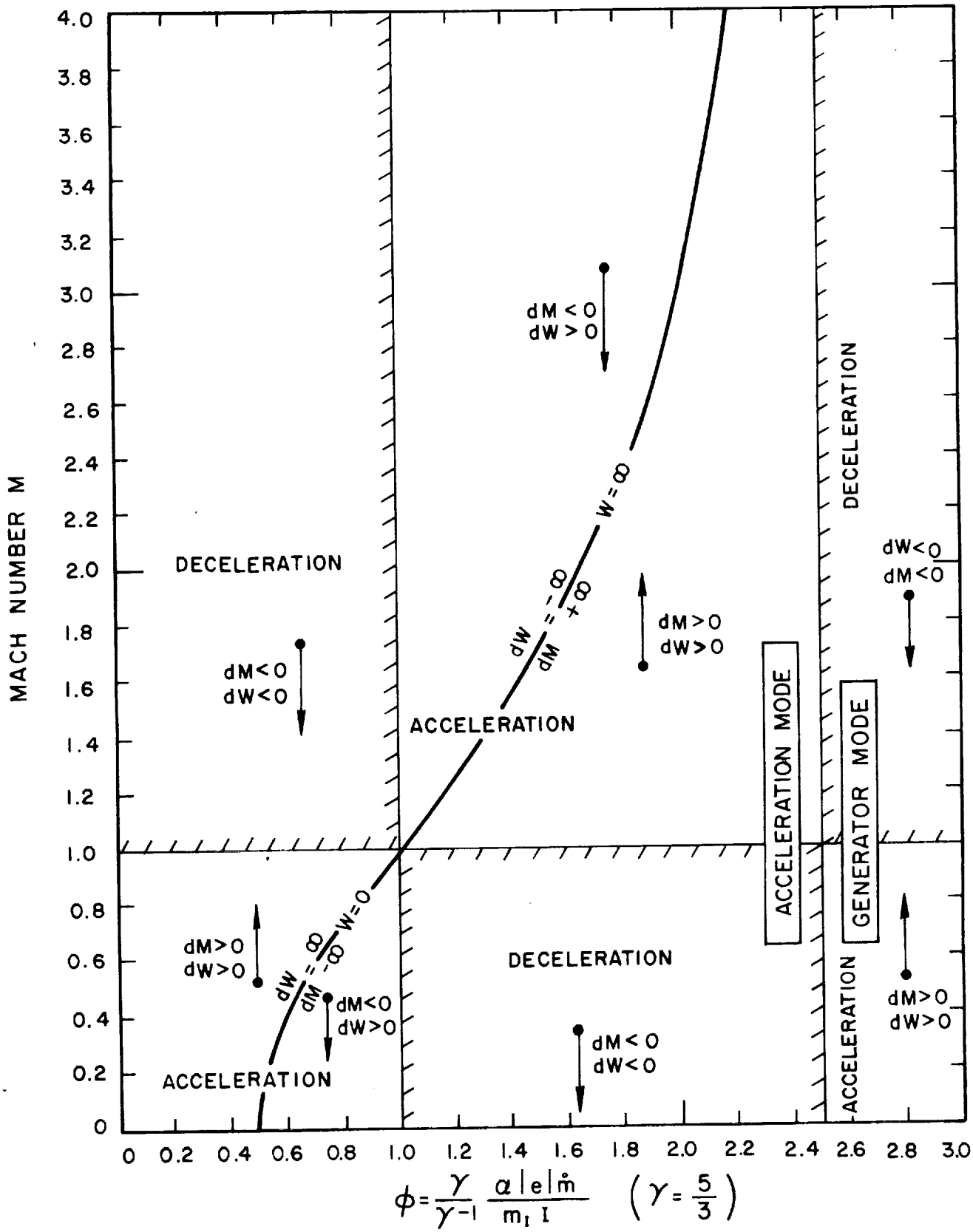


FIG. 2 CHARACTERISTICS REGIONS IN M VS $\phi$ PLANE

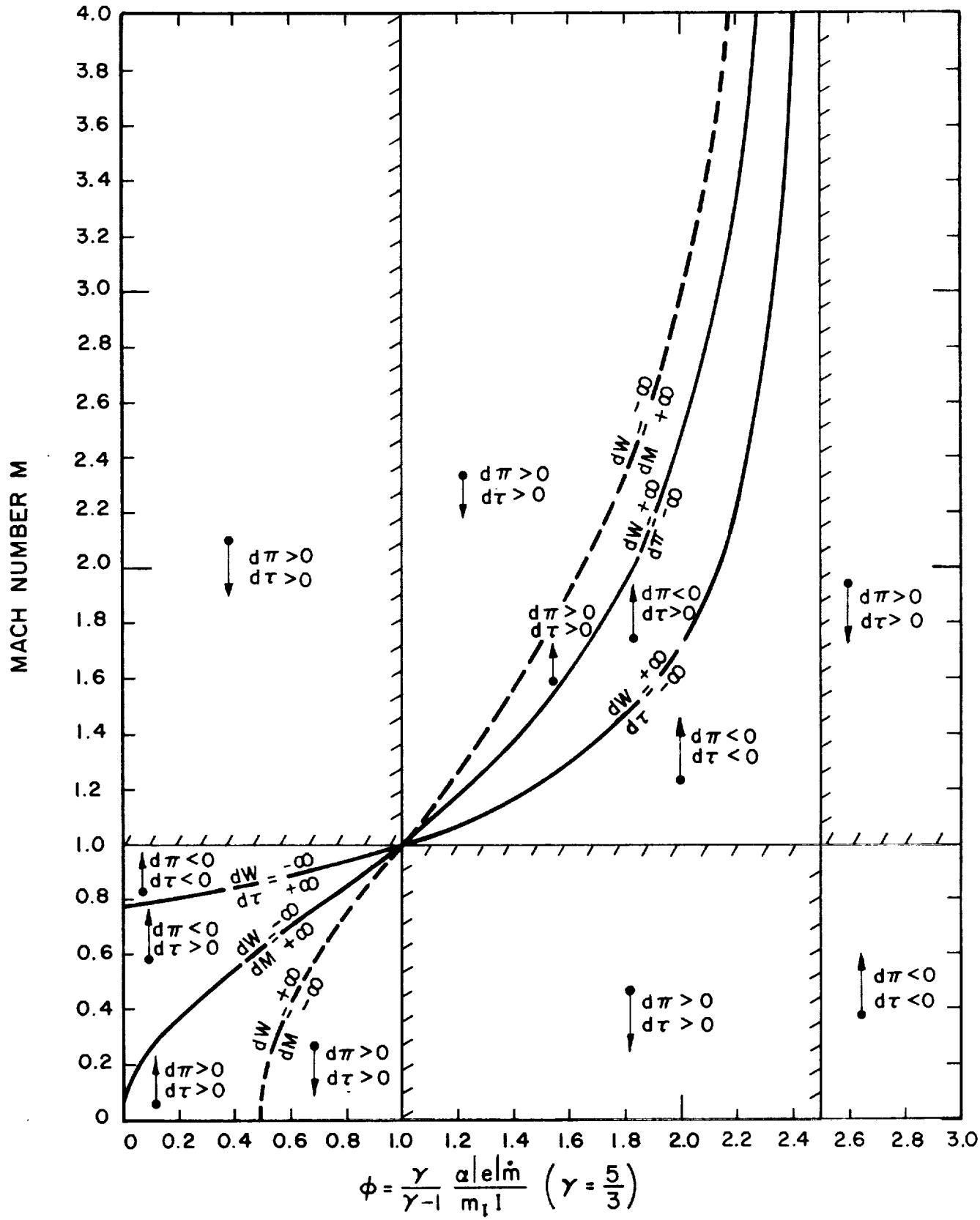


FIG. 3 DISTINGUISHED CURVES IN THE M VS $\phi$ PLANE

$\left(\frac{dW}{d\pi} \to \frac{+}{-} \infty\right)$ AND $\left(\frac{dW}{d\tau} \to \frac{+}{-} \infty\right)$

$$\frac{\Delta S}{R} = \frac{\gamma}{\gamma-1} \ln\left(T/T_o\right) - \ln\left(p/p_o\right) \tag{32}$$

These relations can be used to determine the overall performance capability of the accelerator. Some performance data has been computed and are shown in Figs. 4 to 8. These curves have been evaluated for an inlet Mach number of one, in order to reduce the amount of computation. Data for inlet Mach numbers of greater than one will be computed later. In Fig. 4 the curve along which the inlet and outlet pressure is equal and the curve along which the inlet and outlet temperature is equal are shown. Along the curve of equal inlet and outlet pressure the limit Mach number has been effectively reached. Also, along this curve, the ratio of outlet to inlet temperature is equal to the velocity ratio across the accelerator, hence for high velocity ratios, the gas is raised to a very high temperature at the outlet.

The curves of constant velocity ratio across the accelerator are shown in Figs. 5 and 6. The cross-plot of temperature ratios on Fig. 6 helps to show that it is desirable to operate at fairly high values of the parameter $\frac{}{}$ in order to keep the gas from heating excessively.

The thrust efficiencies obtainable in the accelerator are shown in Fig. 7 and 8. The efficiency $\eta$, shown here is defined as follows:

$$\eta = \frac{\left[A\,(p - p_o) + \dot{m}\,(u - u_o)\right]^2}{2\,\dot{m}\,P} \tag{33}$$

where

A = cross-sectional area of the accelerator channel

P = electrical power input

$\dot{m}$ = mass flow rate of the gas

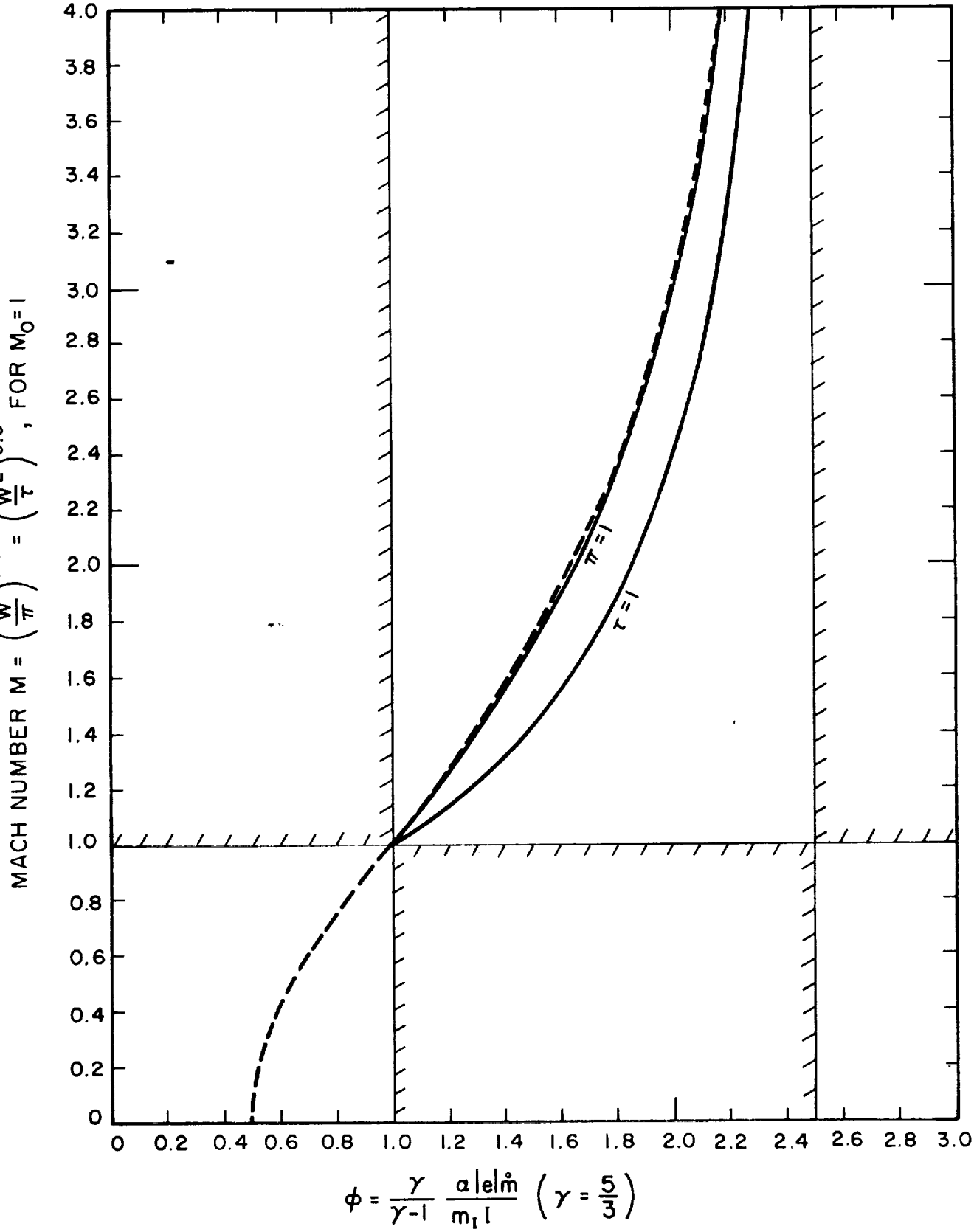


FIG. 4 DISTINGUISHED CURVES IN THE M VS $\phi$ PLANE ($\pi$ = 1) AND ($\tau$ = 1), FOR $M_0$ = 1

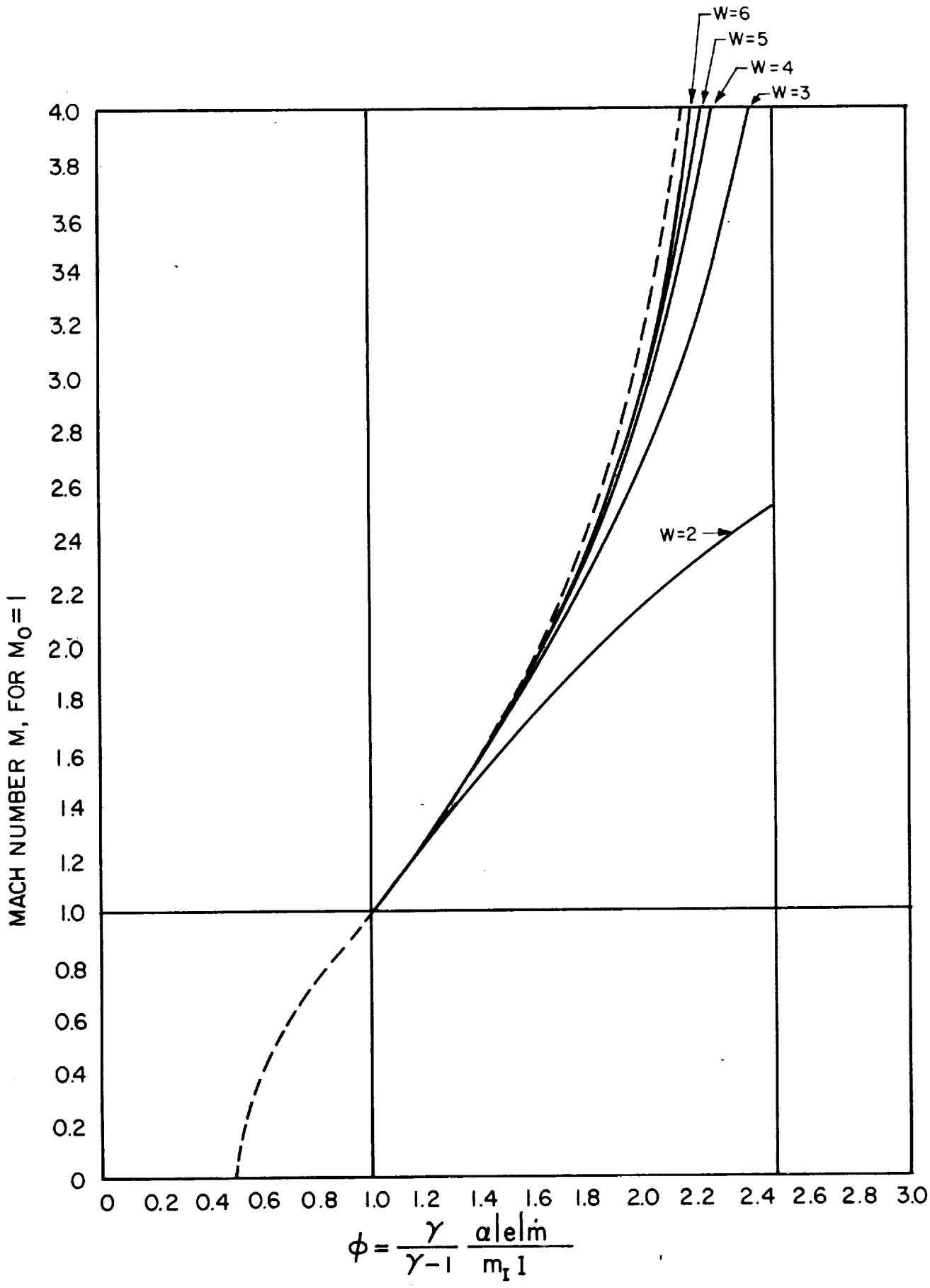


FIG. 5 CONSTANT VELOCITY CURVES IN M VS $\phi$ PLANE

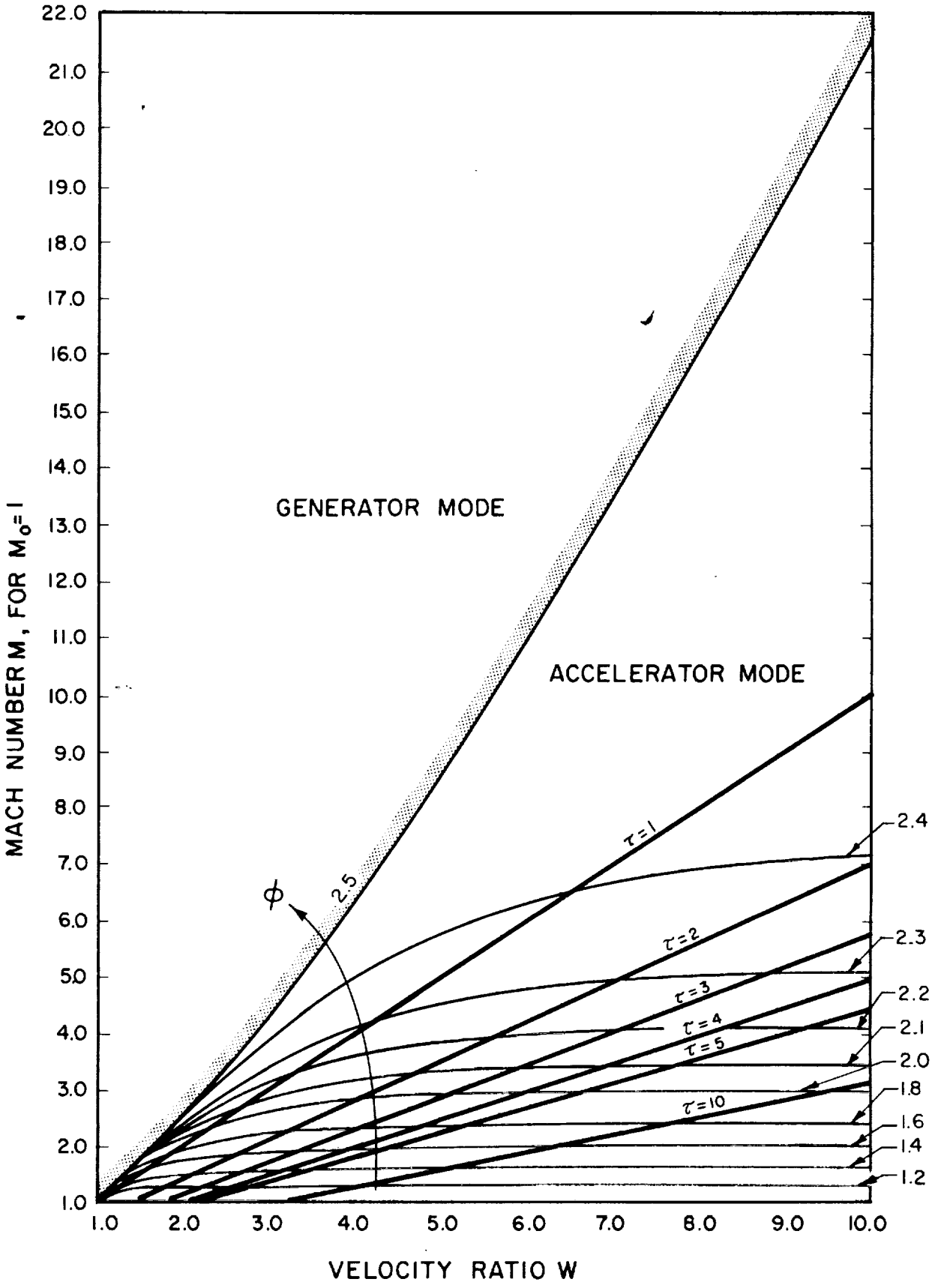


FIG. 6 CONSTANT $\phi$ CURVES IN THE M VS W PLANE

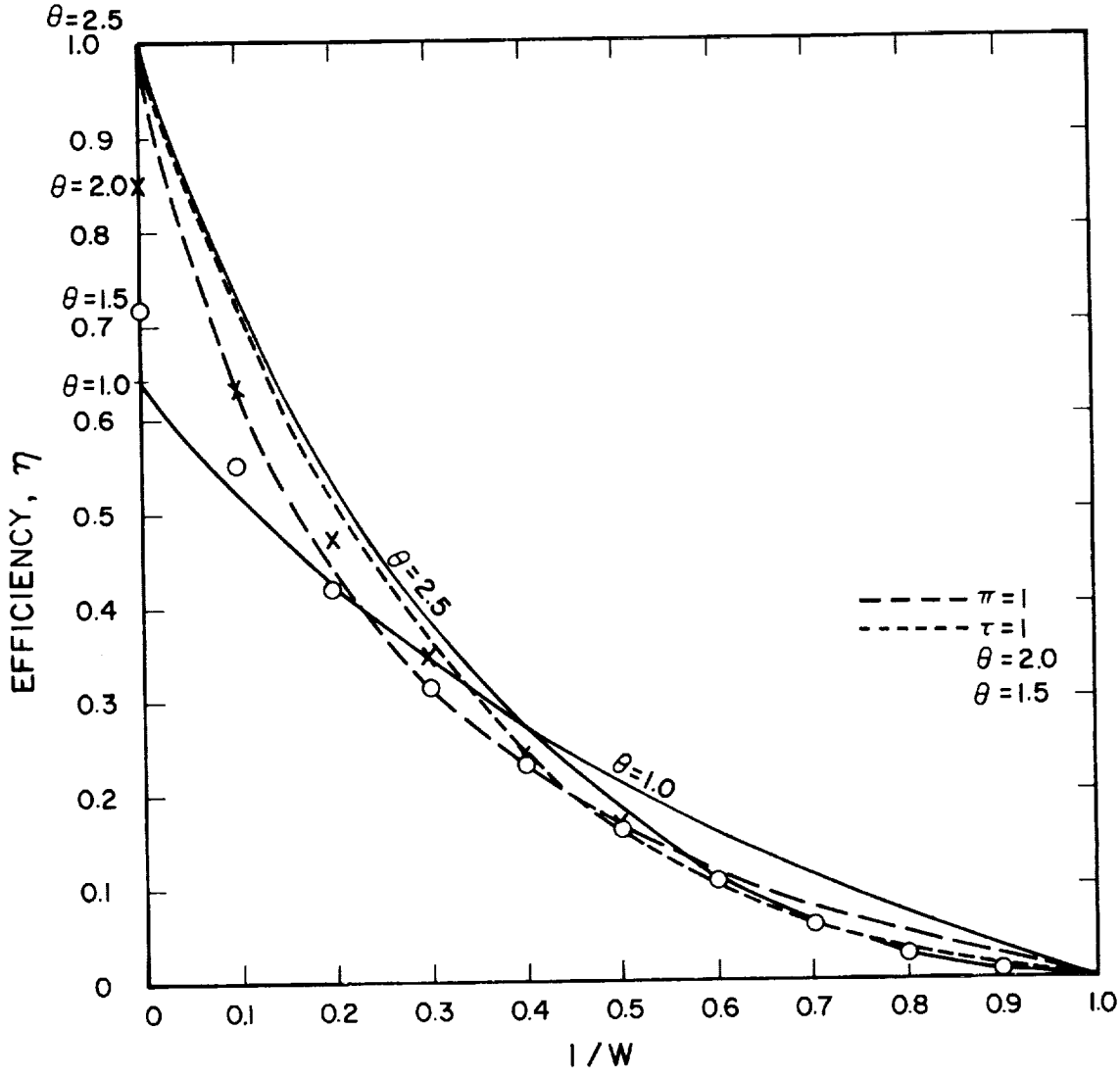


FIG. 7 EFFICIENCY $\eta$ VS W FOR $M_o = 1$

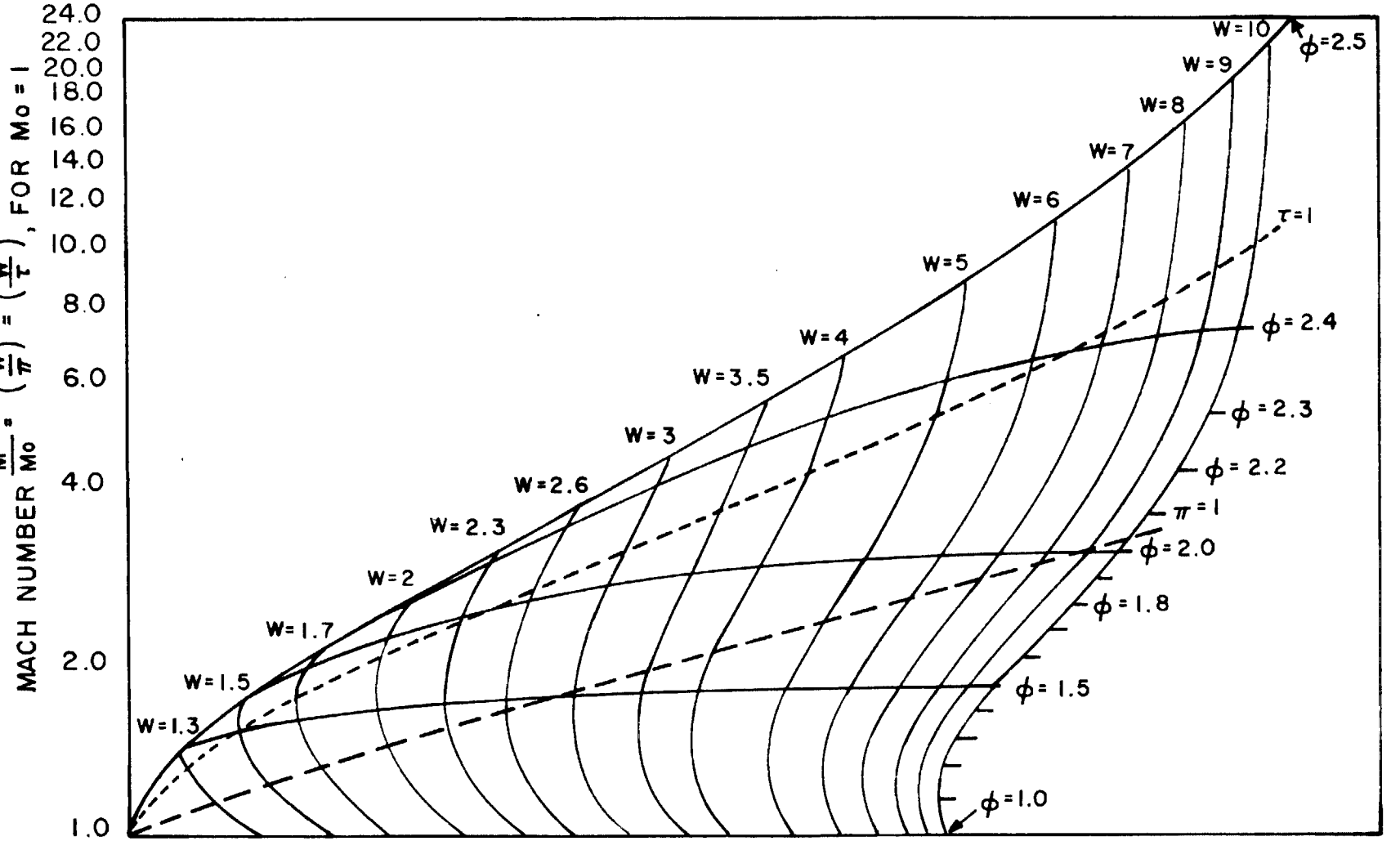


MACH NUMBER AS A FUNCTION OF EFFICIENCY

Fig. 7 shows that the efficiency is primarily a function of the velocity ratio across the accelerator. The curves in Fig. 8 show the relation among the Mach number, the velocity ratio, and the efficiency. Both Fig. 7 and Fig. 8 indicate that it is desirable to operate at high values of the parameter $\psi$ and at high velocity ratios in order to obtain efficiencies of reasonable values (over 60 %).

3.2.4 Determination of the Accelerator Length

The length of the accelerator necessary to obtain a required performance can be obtained from integrating either Eq. (20) or (21). These integrations must be carried out numerically because of the dependence of $\psi_I$ on temperature and density. However, Eq. (21) can be integrated approximately by averaging over the square root of the temperatue on the right hand side of the equation. The result can be expressed as follows:

$$z = \psi^2 \frac{1-\alpha}{1-\psi} \frac{3}{16} \sqrt{\frac{2\pi\gamma}{1+\tau}} \left\{ \frac{2}{\gamma-1} \frac{1}{M_o} (\pi W - 1) + M_o (W^2 - 1) \right\} \frac{1}{n_{Io} q_{Ia}} \qquad (34)$$

This expression indicates that the accelerator length depends primarily on the inverse of the ion-atom cross section times the ion density at the inlet. This is a rather surprising result, in that it shows hthe need for a very long accelerator for a low density gas. In order to obtain a more realistic value for z, the expression shown in Eq. (34) should be multiplied by a factor of 1.5-2.0 in order to account for the cyclic nature of the radial component of the applied magnetic field. An estimate of the value of $n_I q_{Ia}$ needed to keep the value of z below one meter in length can be obtained by putting in some values from the gas dynamic solution.

Put $\psi = 0.80$

$W = 9.0$

$\pi = 1.0$

$\tau = 9.0$

$$\alpha = 0.10$$

$$M_o = 1$$

$$z = \frac{177}{(n_I)_o \, q_{Ia}} \quad \text{meters}$$

For argon at 2,000°K, $q_{Ia} = 70 \times 10^{-20} m^2$, hence to keep the length to about one meter, $(n_I)_o \approx \frac{177}{70} \times 10^{20}$ particle/$m^3$ or $n_o = \frac{11 \times 177}{70} \times 10^{20}$ $= 27.8 \times 10^{20}/m^3$. The actual inlet pressure can be determined to be $p_o = n_o \, kT = 76.7 \frac{\text{newtons}}{m^2} = 7.56 \times 10^{-4}$ atmospheres.

# 4. EXPERIMENTAL RESULTS

## 4.1 Apparatus

After the series of tests of the Hall accelerator which were reported in the First Quarterly Progress Report, the apparatus was disassembled for installation of the magnet force balance. With the force balance installed, the accelerator magnet assembly was independently mounted to the balance platform. The remainder of the system, the arc jet, nozzle, water cooled channel, and the water cooled second cathode were rigidly mounted to the vacuum tank door. This installation is pictured in Fig. 9. It was intended that with this experimental configuration the accelerating magnetic forces, the reaction on the magnet assembly, could be observed and measured.

The force balance was calibrated with the pulley and weight technique and it showed good accuracy and repeatability as long as due care was exercised in aligning the channel and magnet so that no contact between them occurred.

In addition to the force measurements, the heat inputs to the cooling water of the various components were again measured as in the earlier tests.

## 4.2 Test with Cylindrical Configuration

The first tests with the magnet force balance operating were made with the identical accelerator configuration of the earlier tests in order to make a direct comparison of the test results. The results were rather erratic and measured magnet forces were not consistent. In addition, the problem of the current escaping the magnet field by confining itself to the central region of the channel still existed. As a result, it was decided to not continue testing with this cylindrical configuration and to change to an annular geometry.

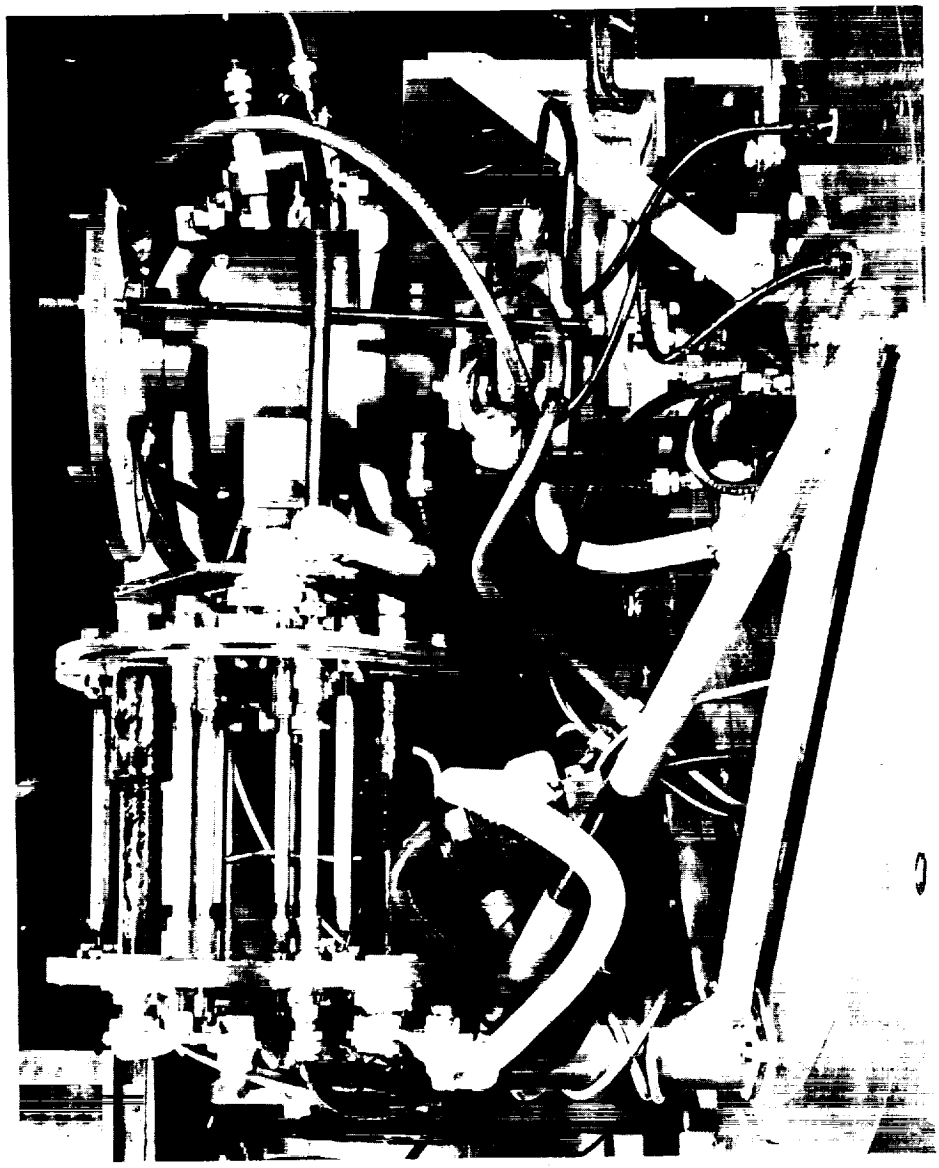

FIG. 9 SIDE VIEW OF HALL ACCELERATOR WITH CYLINDRICAL GEOMETRY. ACCELERATOR MAGNET ASSEMBLY IS MOUNTED ON FORCE BALANCE

### 4.3 Annular Geometry Accelerator

The Hall accelerator was modified by the addition of a 1 inch diameter center-body to the channel as shown in Fig. 10. The radial spacing between the inner and outer cylinders was 0.7 inches. The center-body was supported at its upstream end by three air foil shaped fins within the diverging portion of the nozzle. Cooling water to the center-body was carried to and from the body through these fins. In addition, an uncooled carbon hollow electrode was substituted for the previous water-cooled copper electrode. The hollow electrode was electrically insulated from the water manifold at the downstream end of the outer cylinder.

The center-body contained a core of soft iron to increase the radial magnetic field strength and to decrease its radial gradient. The iron helped considerably and produced the radial magnetic field as mapped in Fig. 11. Unfortunately, the core iron resulted in a pull on the magnet assembly. In addition, magnetic forces were found to exist between the arc jet magnet and the accelerator magnet. The iron was positioned downstream from the center of the magnet assembly to produce a partially cancelling force. Prior to the test runs, the net magnetic pull on the accelerator magnet was determined as a function of magnet current so that corrections to the force balance measurements could be made. The exit momentum target was also used so that the difference between the electromagnetically imparted momentum and that generated by the additional thermal energy input could be determined.

### 4.4 Test Results

Tests were run with the annular geometry using argon as the expellant. Measurements were made of the electrical inputs, cooling water loads and accelerator thrust under test conditions of varying mass flow rate, varying accelerator current with constant magnetic field strength, and varying magnetic field strength with constant accelerator current.

Qualitatively, the results showed that when the accelerator was turned on, but with no accelerator magnetic field on, a 30 to 40 percent increase in jet momentum was measured (depending upon the cur-

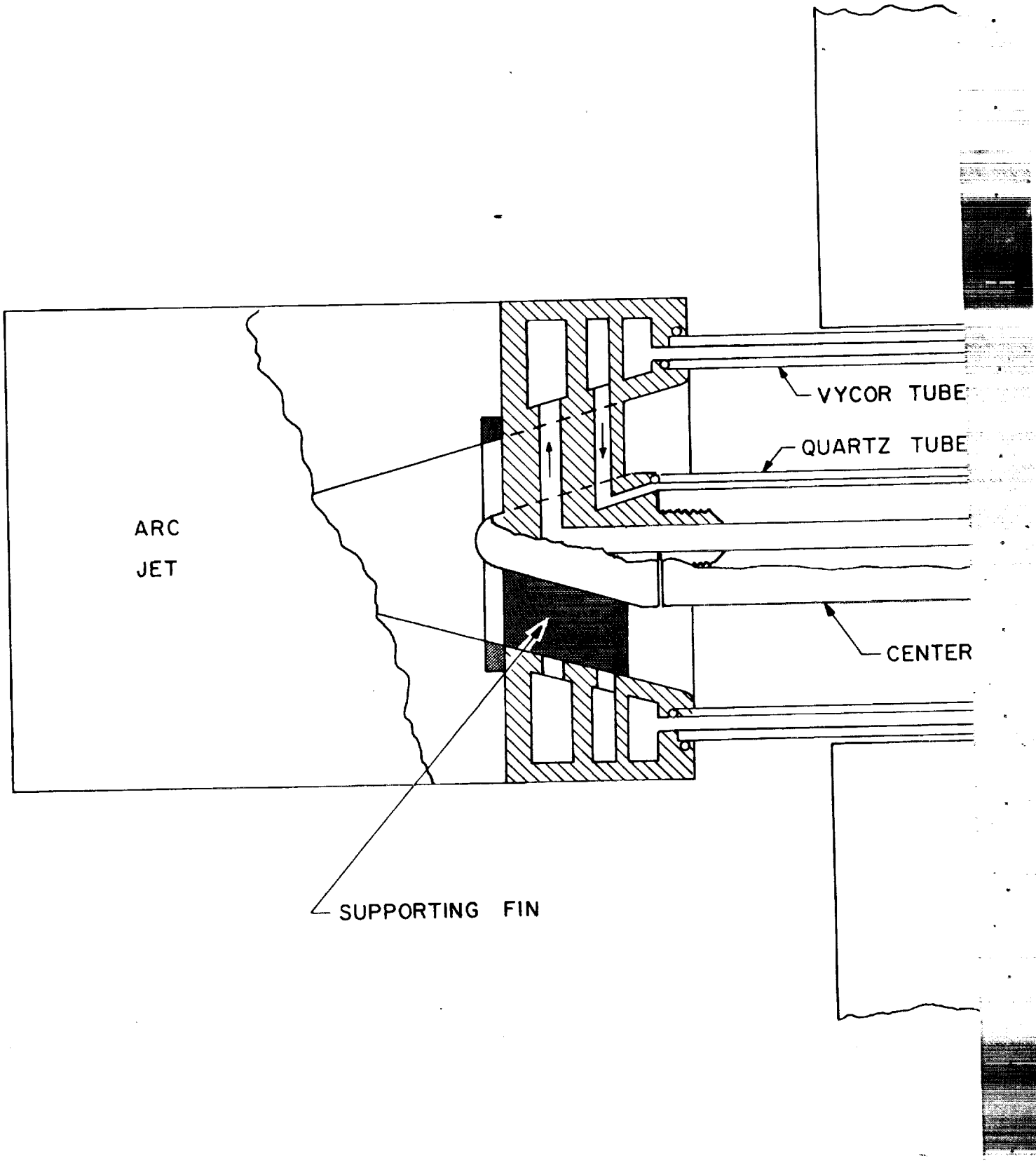


FOLDOUT FRAME

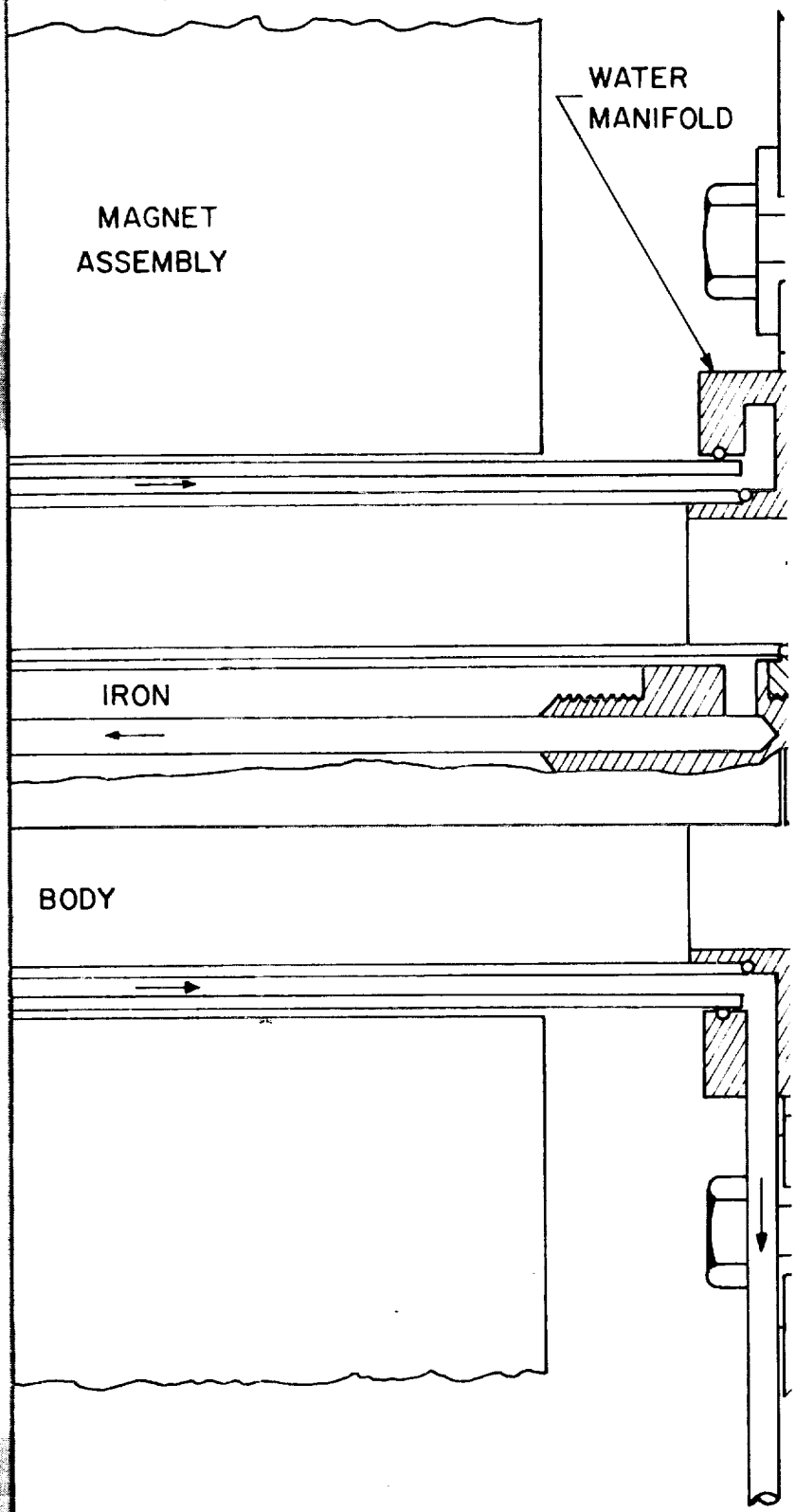


FOLDOUT FRAME 2

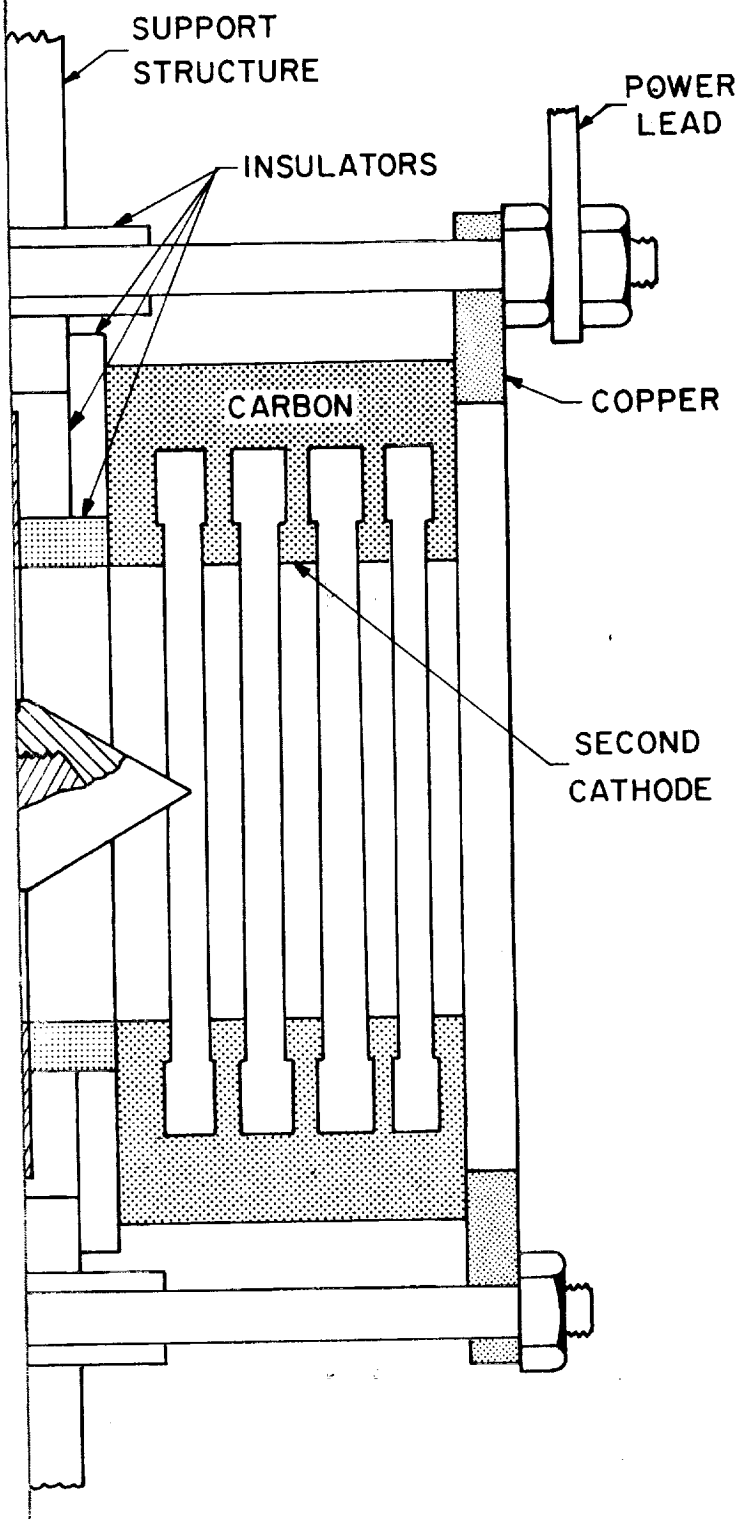


FIG. 10 HALL ACCELERATOR WITH ANNULAR GEOMETRY

FOLDOUT FRAME 3

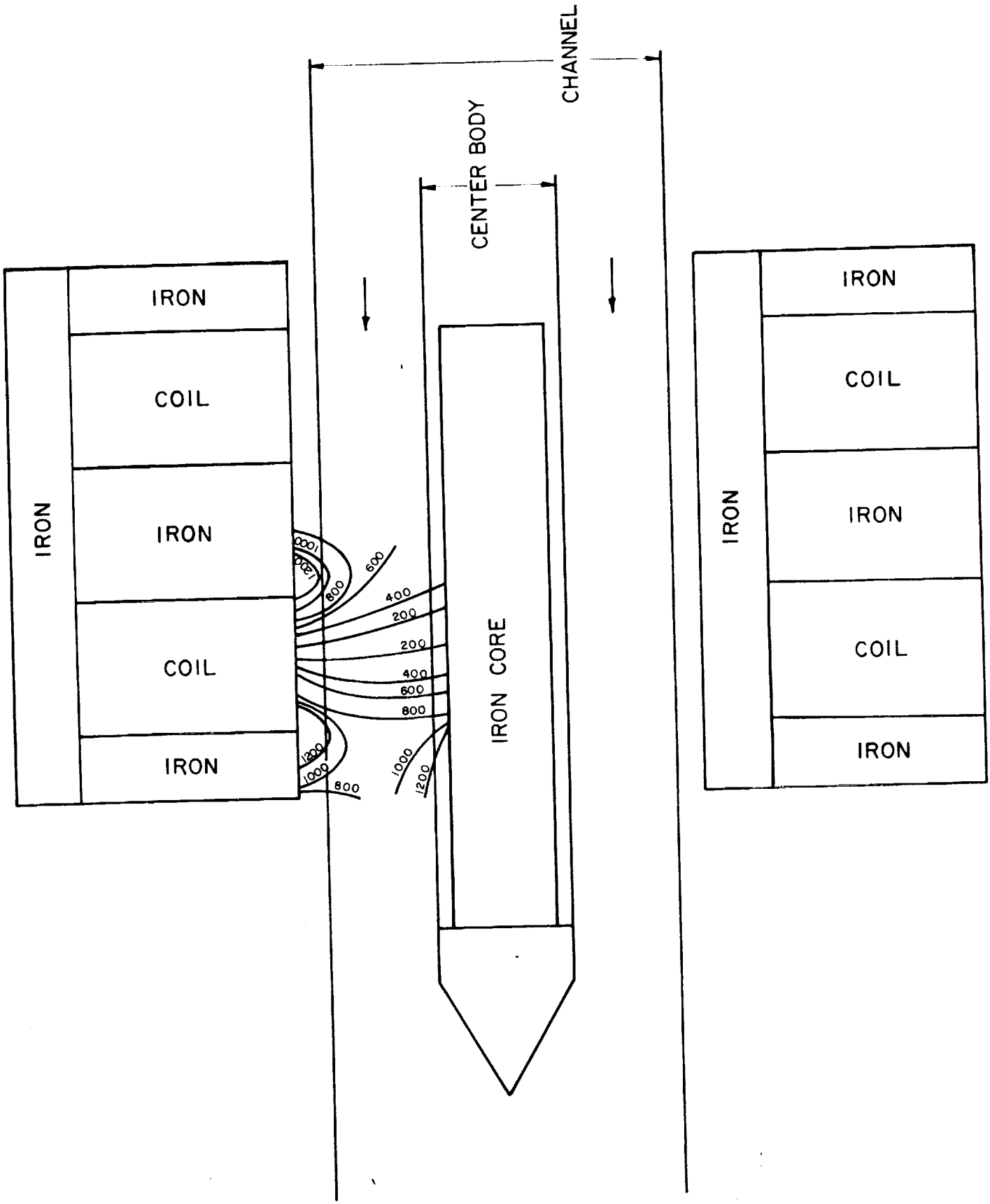


FIG. 11 MEASURED DISTRIBUTION OF RADIAL MAGNETIC FIELD STRENGTH IN GAUSS FOR MAGNET CURRENT OF 1000 AMPS

rent level, gas density, etc.). When the magnetic field was turned on and increased, with the accelerator current being held constant, the thrust increased rapidly at first and then asymtotically approached a maximum thrust increment. When the magnetic field was held constant and the accelerator current increased, a very small increase in thrust was obtained. These results are given quantitatively in the graphs of Figs. 12 and 13. The maximum thrust ratio obtained in these tests was 2.78, i.e., the ratio of total thrust to arc jet thrust.

4.5 Correlation with Theory

On the basis of the experimental data obtained with the annular geometry Hall accelerator, a number of correlations with the theory can be made.

The thrust ratio plotted in Fig. 12 should vary with the applied radial magnetic field strength as described in Eq. (15) which can be written as:

$$X_z = \frac{\frac{\omega_e \tau_e}{B} B^2}{1 + \frac{\omega_e \tau_e}{B} \frac{\omega_I \tau_I}{B} B^2} (j_z - |e| n_I w) \qquad (15a)$$

Under conditions of constant $\omega_e \tau_e / B$, $\omega_I \tau_I / B$, and accelerator current, the relation is of the form

$$X_z = \frac{B^2}{A + CB^2}$$

in which A and C are constants. A curve of this type was fitted to the experimental data and very close correlation was obtained as shown in Fig. 14. The values of the constants A and C are not significant in themselves because the magnetic field strength B is given in terms of the magnet current, but which is directly proportional to B.

Other correlations can also be observed. The thrust as given in Eq. (18);

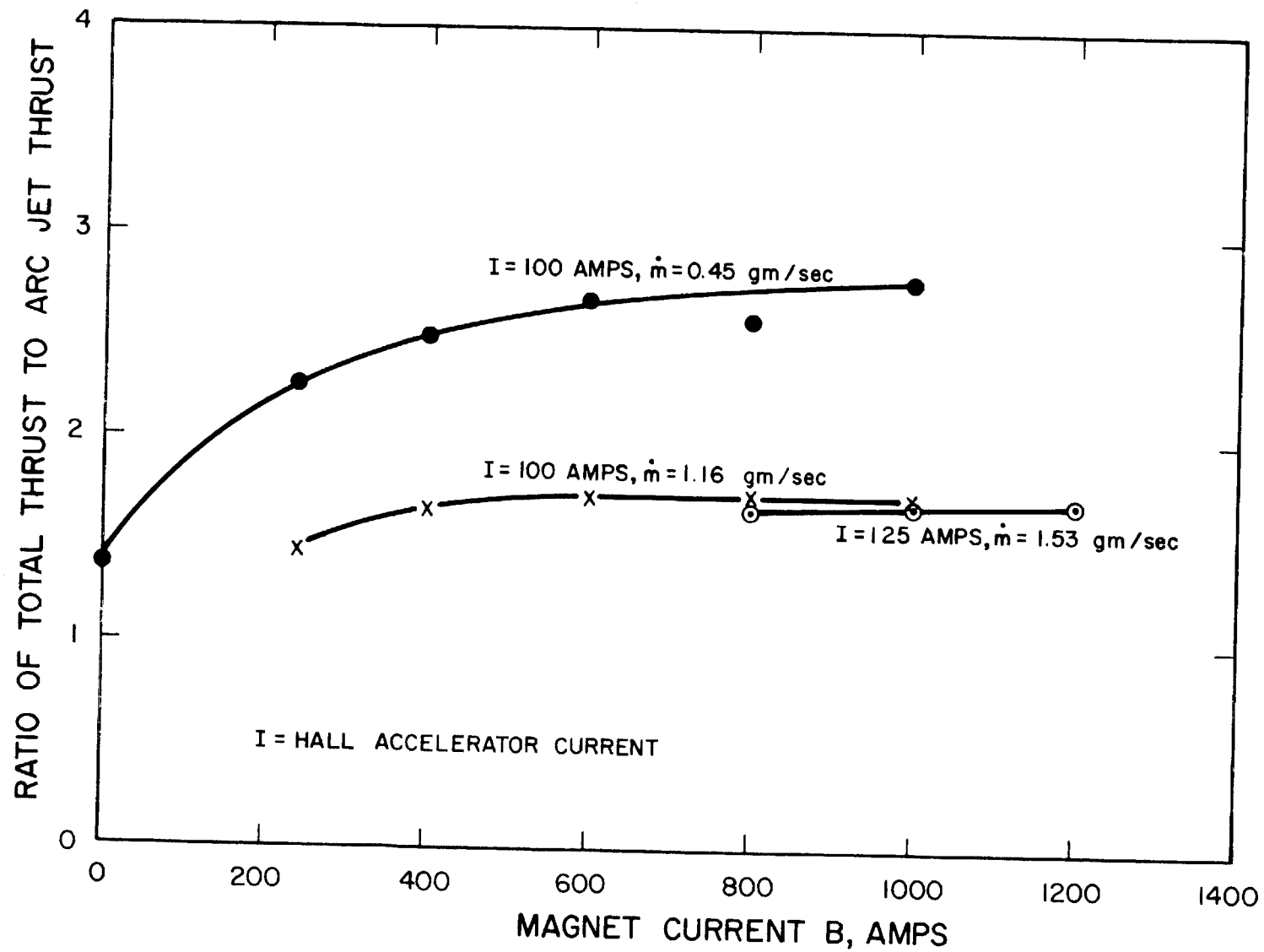


FIG. 12 RATIO OF TOTAL THRUST TO ARC JET THRUST AS A FUNCTION OF ACCELERATOR MAGNET CURRENT

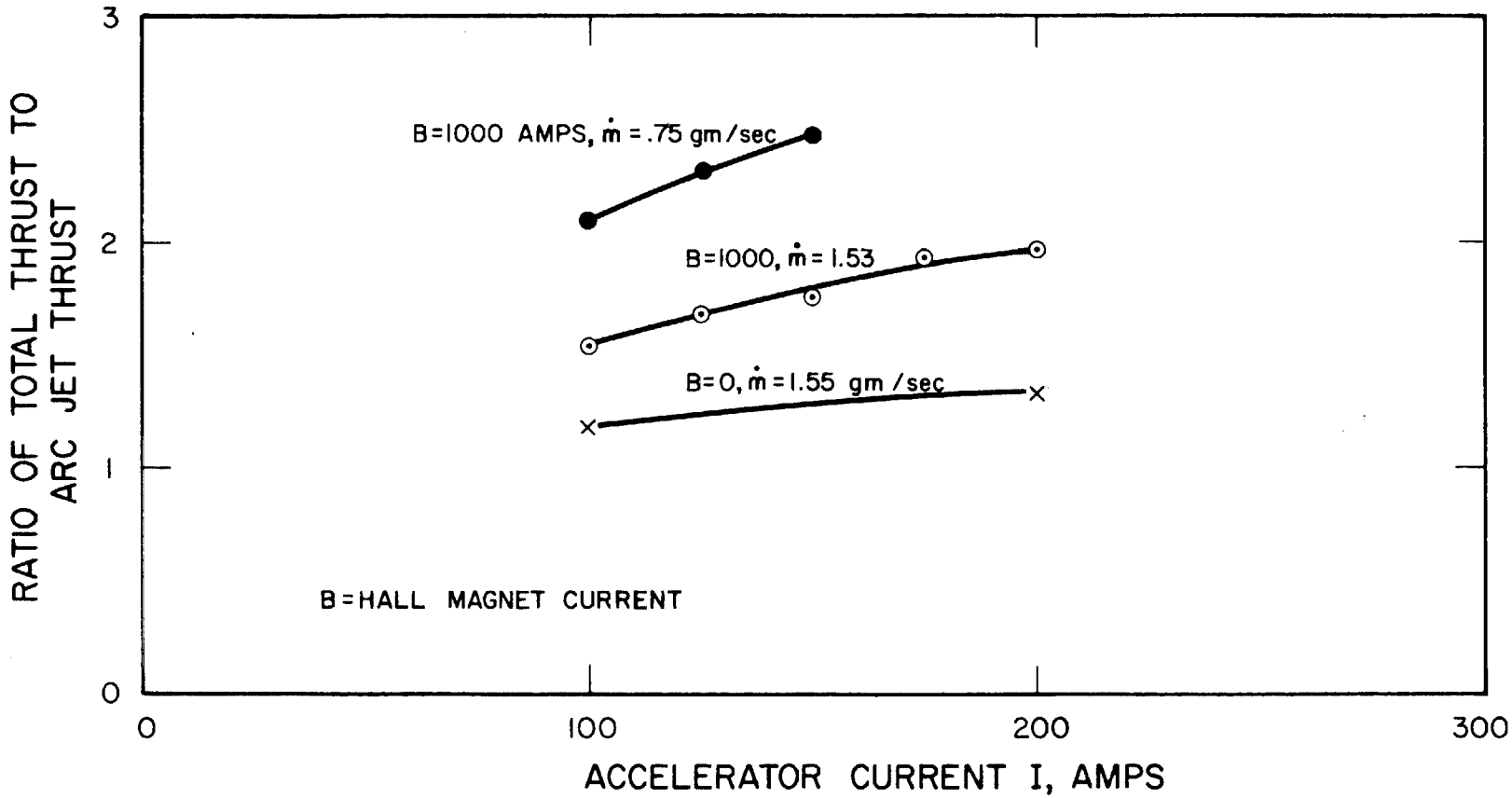


FIG. 13 RATIO OF TOTAL THRUST TO ARC JET THRUST AS A FUNCTION OF ACCELERATOR CURRENT

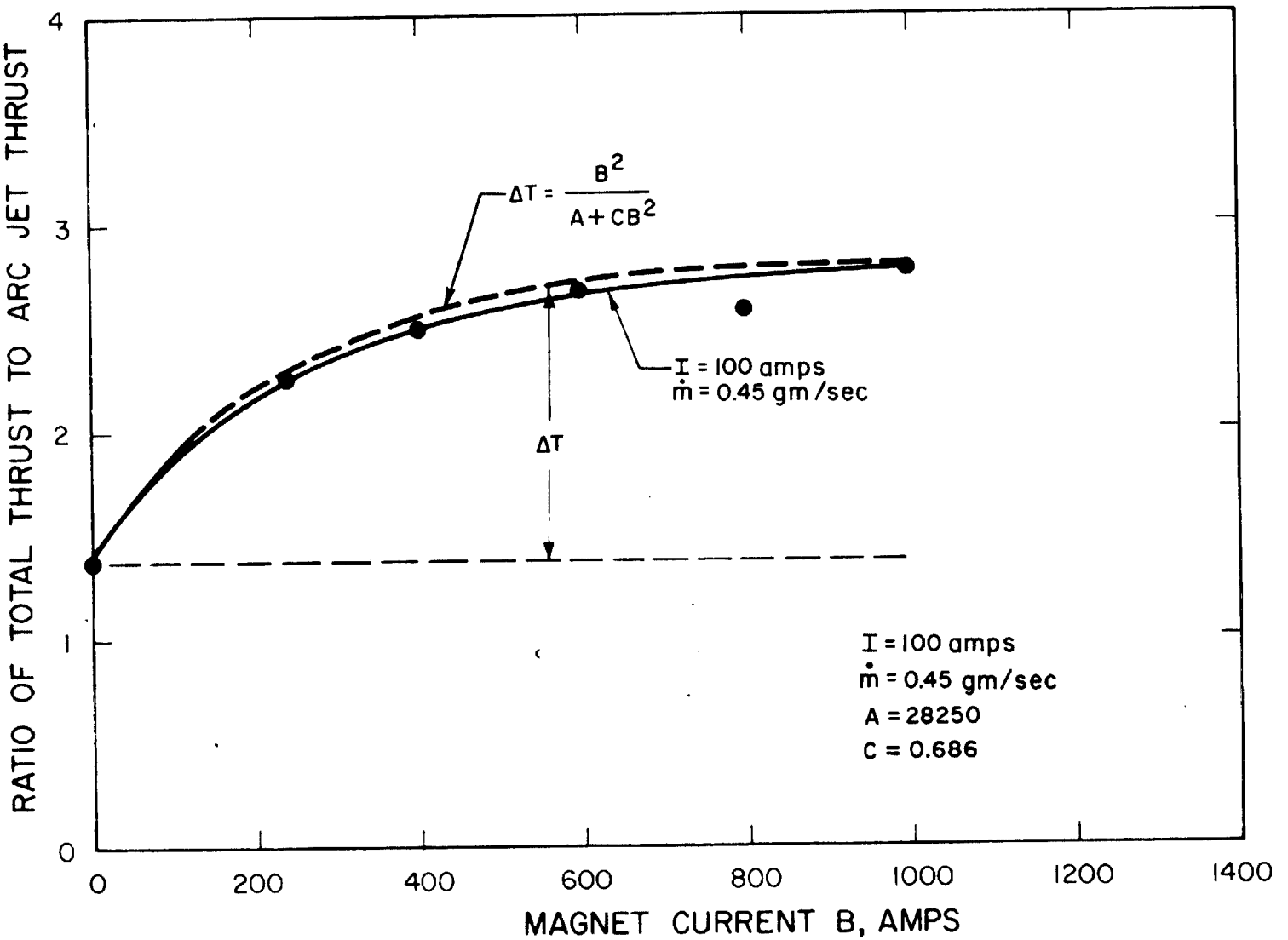


FIG. 14 EXPERIMENTAL DATA AND THEORETICAL CORRELATION OF THRUST RATIO VS ACCELERATOR MAGNETIC FIELD STRENGTH

shows that; 1) as mass flow rate is increased, accelerator thrust should decrease and 2) as current is increased, thrust should again increase. Both of these trends are seen in the data of Figs. 12 and 13. A quantitative correlation cannot be made in this case because the change in the degree of ionization $\bar{\alpha}$ with changing mass flow rate or with current is unknown. However, qualitative agreement between experiment and theory is evident.

## 5. PLANS FOR IMMEDIATE STUDY

### 5.1 Analytical

Further investigations of the gas dynamics of the Hall accelerator will be made. These will include the following:

(1) Investigate the effect of variable ionization level or variable $\psi$ on the properties of the gas dynamic solution.

(2) Evaluate the solution for inlet Mach numbers other than one.

(3) Evaluate the solution for values of $\gamma$ other than 5/3.

(4) Devise solutions for a constant pressure acceleration (variable area).

(5) Devise solutions for constant temperature acceleration.

The studies to determine the energy and momentum loss due to thermal conduction and wall friction will be continued. These studies should help to determine an optimum configuration for a high specific impulse, fairly high efficiency accelerator.

### 5.2 Experimental

Further studies will be carried on with the hollow cathode to try and obtain a uniform current density distribution over the surface area.

The entire unit, both arc jet and accelerator will be redesigned using our recent analytic results in order to try and obtain an $I_{sp}$ of 2,000-3,000 sec and an efficiency of over 50 $^{o}$/o.

Modifications are now being made to the tank so that probes can be introduced into the exhaust jet in order to try and measure the stagnation pressure and the flow Mach number.

6. EXPENDITURE REPORT

Manhour Expenditure of Scientific Personnel of the Quarter of 17 August to 16 November 1962

| Man | Labor Hours | Contribution |
|---|---|---|
| E. Baum | 144 | Calculation of gas properties. |
| R. Buhler | 32 | Technical discussion on balance design. |
| G. Cann | 168 | Overall supervision of project and theoretical analysis. |
| L. Gallagher | 128 | Instrumentation of experiment. |
| G. Marlotte | 116 | Theoretical analysis. |
| R. Moore | 42 | Design of balance. |
| R. Pritchard | 204 | Design and fabrication of experiment. |
| J. Teem | 4 | Technical discussions. |
| R. Ziemer | 308 | Theoretical analysis, calculation of gas properties, experimental analysis. |

CONTRACT NO. NAS 3-2500

CUMULATIVE FUNDS PROJECTION
(INCLUDES COST, COMMITMENTS AND FEE)

BASIC CONTRACT $ 124,973
START 17 MAY 1962

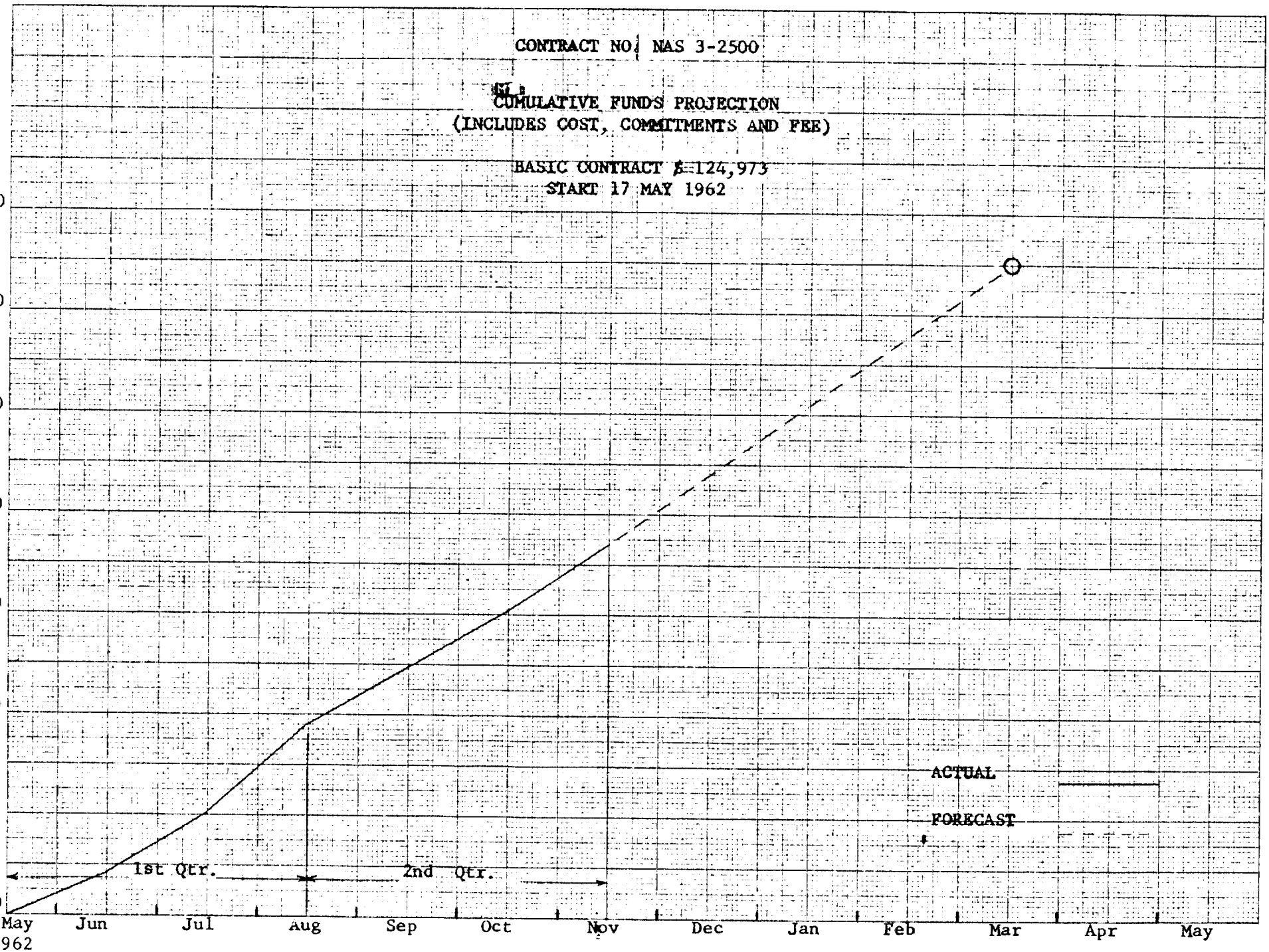

## REFERENCES


1. G.L. Cann, R.D. Buhler, J.M. Teem, and L.K. Branson; Magnetogasdynamic Accelerator Techniques, Final Report, Contract No. AF 40 (600)-939, Arnold Engineering Development Center, Tennessee, November 1961.

2. G.L. Cann; Energy Transfer Processes in a Partially Ionized Gas, Memorandum No. 61, Guggenheim Aeronautical Laboratory, California Institute of Technology, June 15, 1961.

3. 3160 First Quarterly Report, 17 May 1962 to 17 August 1962, Contract NAS 3-2500, for NASA, Lewis Research Center, Cleveland, Ohio.